

RSC Advances



This is an *Accepted Manuscript*, which has been through the Royal Society of Chemistry peer review process and has been accepted for publication.

Accepted Manuscripts are published online shortly after acceptance, before technical editing, formatting and proof reading. Using this free service, authors can make their results available to the community, in citable form, before we publish the edited article. This *Accepted Manuscript* will be replaced by the edited, formatted and paginated article as soon as this is available.

You can find more information about *Accepted Manuscripts* in the [Information for Authors](#).

Please note that technical editing may introduce minor changes to the text and/or graphics, which may alter content. The journal's standard [Terms & Conditions](#) and the [Ethical guidelines](#) still apply. In no event shall the Royal Society of Chemistry be held responsible for any errors or omissions in this *Accepted Manuscript* or any consequences arising from the use of any information it contains.

ARTICLE

Three Dimensional (3D) Flexible Graphene Foam/Polypyrrole Composite: Towards Highly Efficient Supercapacitors

Cite this: DOI: 10.1039/x0xx00000x

Sakineh Chabi,^a Chuang Peng,^b Zhuxian Yang,^a Yongde Xia,^a Yanqiu Zhu*^aReceived 00th January 2012,
Accepted 00th January 2012

DOI: 10.1039/x0xx00000x

www.rsc.org/

Polypyrrole (PPY) functionalized 3 dimensional (3D) graphene foam (GF) with remarkable electrochemical performance has been synthesized in this work. The resulting 3D PPY-GF electrode is free standing and hence was used directly as working electrode without using any binder or carbon additives. The unique features of the PPY-GF composites such as their hierarchically flexible 3D network, and high conductivity of p-doped PPY, afforded PPY-GF electrodes with enhanced pseudocapacitive properties. Under optimal conditions, a maximum specific capacitance of 660 Fg⁻¹, specific energy of 71 Whkg⁻¹, comparable to battery performance, and a specific power of 2.4 kWkg⁻¹ (at 0.5 mA) were obtained. Both GF and PPY-GF electrodes exhibited an excellent cycle life and retained almost 100% of their initial capacities after 10,000 and 6,000 charge-discharge cycles, respectively. This highly enhanced stability is attributed to the significant impact of the GF density on the flexibility of the electrode, and the hierarchical pore structures which provided short effective pathways for ion and charge transportations and stayed unchanged after thousands of cycles. The PPY-GF pore size varies from a few nm for small pores to a hundred of μm for macropores.

Introduction

Supercapacitors are considered as one of the most important energy storage devices (ESDs), since they hold the hope of achieving battery-like specific energy along with capacitor-like specific power. Towards the ultimate goals of harnessing high capacity, high specific energy (Whkg⁻¹), high specific power (Wkg⁻¹) and good cycle life (10,000 cycles) for the next generation of electrochemical ESDs, numerous architectures and a wide range of composite materials have been investigated to date. One of the most promising structures that have been proposed is the three dimensional (3D) architecture.

3D electrodes, 3D current collectors, full 3D batteries (e.g. interdigitated, trench, and concentric designs), 3D micro and nano batteries and 3D supercapacitors have been the subject of recent intensive studies, whereas 3D electrodes have been the core of such research.¹⁻⁶ 3D electrodes have recently been deployed for battery, supercapacitor, fuel cell, and solar cell applications and to date very good results have been reported.^{4,6-12} Fast charge-discharge rate for

battery devices,^{4, 6-10} and improved energy for supercapacitors have been the two key advantages of 3D electrodes.^{11, 12}

In a 3D electrode, the electroactive materials do not suffer from the high trade-off between the power and the energy as they do in a traditional plane electrode, since the third dimension allows for storing more energy without the need of increasing the thickness of electroactive materials, thus the specific power is less compromised.¹³⁻¹⁷

Owing to various features of 3D architecture, this concept can be deployed differently in order to contribute more efficiently to the final performance of the electrode and device. One interesting approach is to use 3D graphene (GF) or its derivatives to produce graphene-based composites. Depending on the demanded properties of the composite such as its shape, flexibility, hierarchical structure, stability and desired density, these aspects can be achieved by introducing them in the GF scaffold since it is more convenient to engineer GF rather than their composite.

Different forms of carbon including graphene, graphite, carbon nanotube (CNT), and their monolith composites have been the main materials for capacitor electrodes. However, pure carbon is incapable of providing the desired energies in supercapacitors. That is due to a variety of reasons including: non-faradic storage mode, low capacity, π - π stacking in few layer graphene, large inaccessible surface area of graphene, intrinsic microstructure of the carbon and etc. Regarding all the electrochemical limitations of carbon materials it would be highly desirable to introduce electroactive materials into a 3D graphene network.

Apart from the main advantages of the 3D structures which have been discussed earlier, the hierarchical feature of a GF scaffold can also help in stabilizing the surface morphology of the redox counterpart, as the pores can function as a host to the redox elements and accommodate the strains in the entire electrode structure during cycling.^{5, 18, 19}

So far, conductive polymers and transition metal oxides have been the traditional partners for carbon materials. Conducting polymers such as Polypyrrole (PPY) and Polyaniline (PANI) are promising pseudocapacitive electrode materials for supercapacitor applications. They are inexpensive, environmentally friendly, highly conductive in doped states, easy to synthesis from both aqueous and non-aqueous solvent, and also benefit from the fast doping/un-doping process. However, conductive polymers such as PPY, which is of special interest in this context, suffer from low mechanical stability and pulverization during the repeated charge-discharge process, and they lose more than 50% of their initial capacitance after only a few hundreds of charge-discharge cycles.²⁰⁻²³

To improve the cycle life of the electrodes, PPY can be incorporated into a strong and conductive 3D matrix, to form composite electrodes. CNTs, carbon nanofibers, graphene foams, graphene oxides, reduced graphene oxide, and 3D macroporous carbons are all good candidates for making such PPY composite electrodes, and many researches have been conducted in this field.^{20, 24-31} Although improved cycle life have been reported so far, the specific capacity values of most of them are still not high enough, falling below 400 Fg^{-1} , and importantly the cycle life rarely reaches thousands of cycles, lagging behind the market demand.^{20, 25, 27, 29-31} Indeed, the full advantages of an ideal 3D architecture have not been deployed properly, as these reports are mainly limited to the improvement of only one or two criteria (energy enhancement or power improvements). We believe that an advanced 3D structure can contribute more to the device efficiency. For instance, capacitor-like cycle life, high flexibility, higher energy values, binder free structure are all achievable in the optimum 3D structure.

In the present study we demonstrate that by using a highly flexible 3D GF as a scaffold, a 3D PPY-GF composite electrode can be created which exhibits significantly improved electrochemical performance.

Results

PPY-GF composites were prepared by a two-step process, chemical vapour deposition of the GF followed by oxidation polymerization of pyrrole on the GF scaffold. By slightly modifying the chemical vapour deposition that was first reported by Chen et al,³² we have succeeded in producing one of the lightest GFs. Using the mass-dimension data of various samples, we obtained an average value of

3 mg cm^{-3} as the bulk density of the resulting GFs. The as-grown GFs were prepared directly without using PMMA, as the prepared GF was strong enough to withstand the etching process of Ni foam. Figure S1, illustrates the preparation procedure of the GFs and PPY-GF composites.

Figure 1 shows the SEM images and EDS results of the GF, PPY and chemically polymerized PPY-GF. Figure 1a is a 3D image of the as-prepared GF. The GF copied and inherited the interconnecting feature from its parental 3D Ni template. The flexibility of the foam is demonstrated in Figure 1b, as the GF can be bended largely by a pair of tweezers. EDS analysis (Figure 1c) only shows the C signals in the spectrum, confirming a complete Ni template removal during etching process. The low magnification image (Figure 1d) revealed an average of 200 μm for macro pores; and a few nm pores were characterized at high magnification.

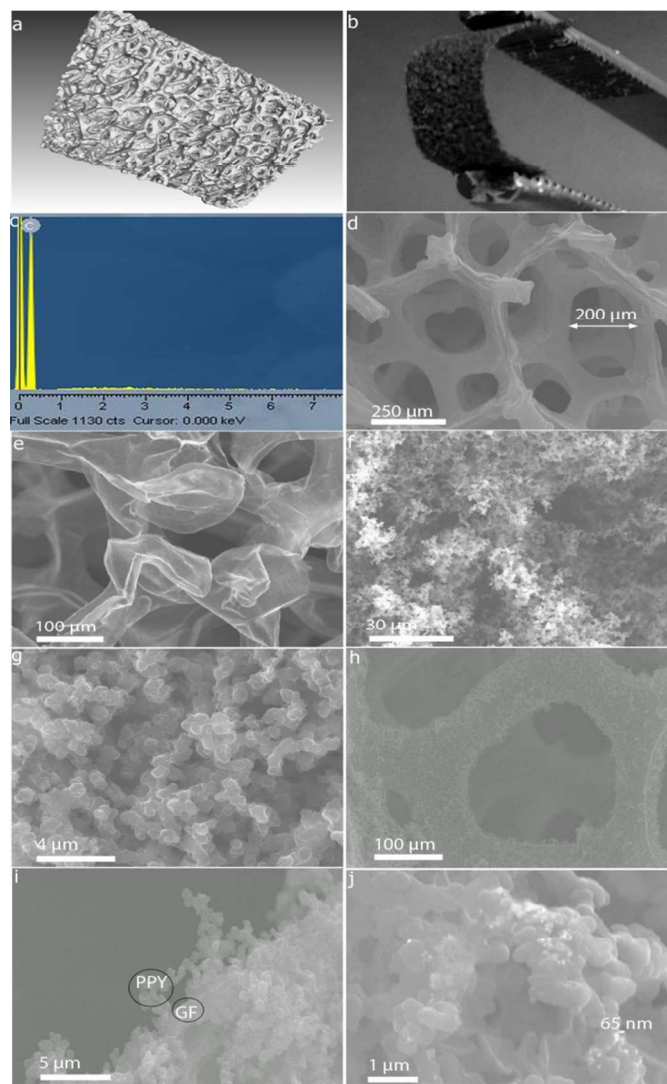


Figure 1: A 3D image of the GF (a), a photograph of the bended GF (b), the EDS spectrum of the GF (c), SEM images of GF (d, e). The arrow in image (d) shows a macropore with 200 μm in size. SEM images of the PPY (f, g) and PPY-GF (h-j).

PPY images are presented in Figures 1f and 1g. Polymer aggregation is visible in the images. In contrast, the PPY were coated uniformly on the surface of GF substrate (Figure 1h-j), and the PPY-GF

composites maintained the same interconnected 3D structures as in the GFs. At different magnifications (Figure 1d-1j), the SEM analyses revealed a wide range of pores in the 3D PPY-GF composites, from 10s nm to 100s μm . Partly, the hierarchical characteristic of the composite is inherited from the GF scaffold. It is noted that the PPY-GF exhibited relatively smaller pore sizes than that of pure GFs, due to the PPY deposition. XRD profiles of the GF, PPY and PPY-GF are presented in Figure S2.

The thermal behaviour of different samples was studied by the TGA method. Figure S3 shows the TGA results of the GF-Ni and GF. The TGA profile of the PPY-GF composite against GF and PPY is shown in Figure 2. As seen from the graph, the PPY loses its weight completely at about 450°C, while there is a minimal weight loss for GF at the same temperature. Accordingly, a 65% weight loss in the PPY-GF composite at that temperature indicates a 35% PPY content in the composite.

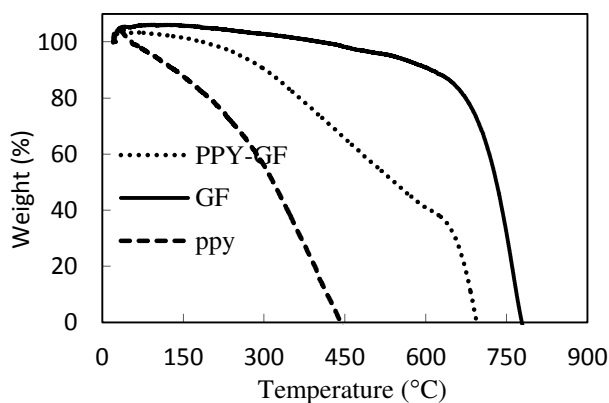


Figure 2: TGA profiles of different samples.

Figure 3 displays the Raman spectra of the GFs, PPY and PPY-GF composites. For the GF, two main peaks appeared at about 1572 cm^{-1} (G) and 2750 cm^{-1} (2D). The G band is the E_{2g} mode of graphene and is related to the in-plane stretch vibration of C=C pair. The 2D mode is the two phonon bond and is activated by the double resonance at the zone boundary.^{2,3} The absence of D mode (at about 1300 cm^{-1}) is indicative of the good crystal structural feature of the foam, as well as its monolithic carbon character. Depending on the number of graphene layers, the G peak position can be shifted towards higher or lower wave frequencies, however its shape remains un-affected by the number of graphene layers.⁴ The spectra of the PPY-GF composite samples showed a combined feature of both GF and PPY. The PPY peaks appeared in the range of 800-1000 cm^{-1} , representing the N-H and C-H deformation of the Pyrrole ring and attributed to the GF contribution. Its G peak appeared at about 1577 cm^{-1} and slightly shifted to upper wavenumbers, accompanied by the gradual disappearance of the 2D band, due to the PPY formation on the GF surface.

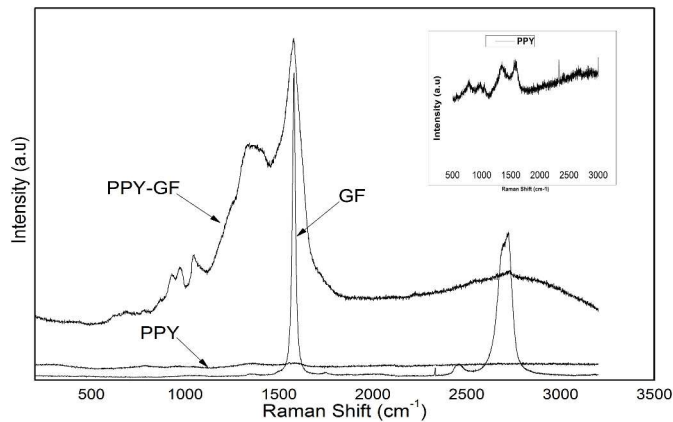


Figure 3: Raman spectra of the GF, PPY and PPY-GF. The inset is the enlarged Raman spectrum of the PPY.

Figure 4 shows the TEM images of the GF (Figure 4a) and the PPY-GF composite. The as-prepared GF contains flakes with different numbers of graphene layers (Figure 4b), from only 2-3 layers in some flakes to > 20 layers in others. These findings are consistent with the Raman analyses and the XRD calculation. The PPY coating is clearly visible in the TEM images of the PPY-GF composite. Based on Figure 4c-4f, we have estimated that the PPY chain diameter is 14 nm (Figure 4e). Figure 4f shows the cross-section of another part of the PPY-GF composite, revealing an interlayer distance of 0.34 nm for the GF. The related flake consists of only 4 graphene layers.

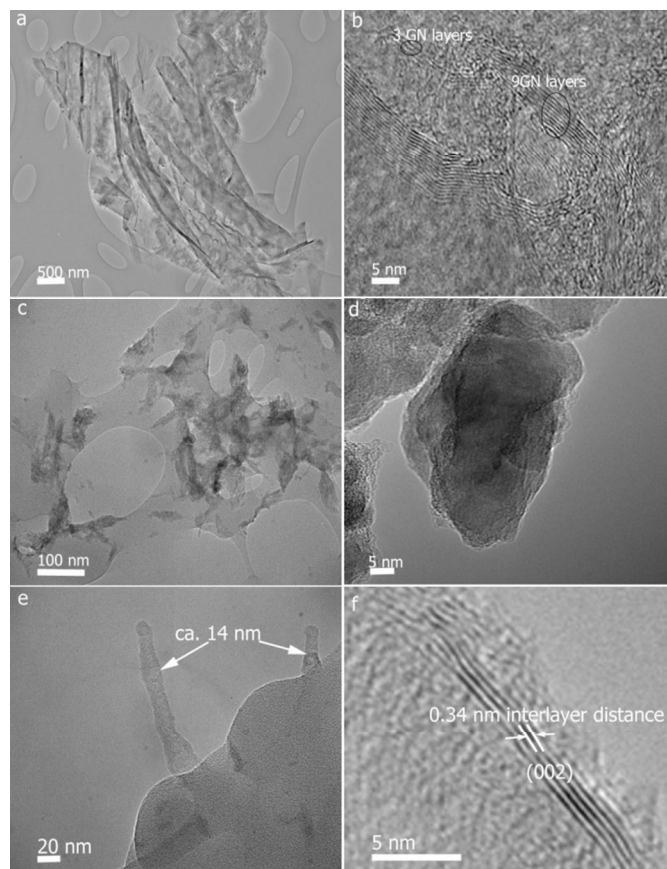


Figure 4: TEM images of the GF (a, b) and PPY-GF(c-f). The pointed fibers in (e) have a diameter of ca. 14 nm

The tensile test results of the GFs are shown in Figure 5. For our specimens (length \times width \times thickness = $5 \times 2 \times 1.5$ mm) with a gauge length of 2.3 mm and under a load of 0.04 N, a 25% strain was recorded. No breakage was observed up to 75% strain. The small but consistent noise in the signals in Figure 5b is believed to arise from contributions of some breaking layers of graphene during pulling. A gradual progression in fact allows for the majority of layers in the network maintaining the integrity of the foam, even after the breakage of some layers. The detailed study for the mechanical behaviour of the GF will be reported separately later. Moreover the GFs also showed a very good consistency under compression tests and achieved a maximum compression of 80% under a load of 0.025 N. Thus, the GFs exhibit very good mechanical performance in compressing, stretching and bending (Figure 1b) tests, all pointing to their suitability as candidates for 3D ESD electrodes, whose performance have been assessed using a three electrode cell in a 0.5 M KCl electrolyte.

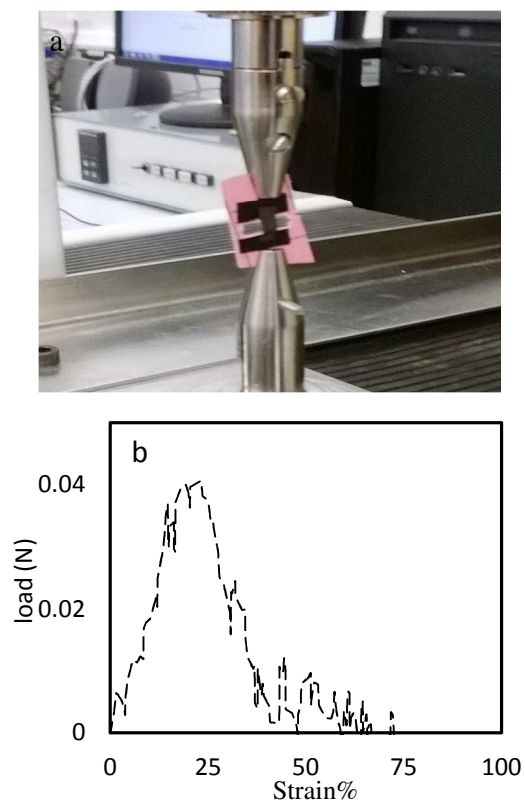


Figure 5: A photograph of the GF during mechanical test (a), and the load-strain curve of the GF (b).

Figures 6a and 6b show the cyclic voltammetry (CV) curves of the GFs obtained at a scan rate of 0.1 Vs^{-1} . The rectangular shape shows the typical behaviour of double layer capacitors. The straight lines at both ends of the CV curve represent a fast charge-discharge process at the foam and are indicative of the quick diffusion of the electrolyte into the GFs. The stability of the GF electrodes was assessed by running repeated CV tests for a longer time. As shown in Figure 6, the first and 10,000th cycles almost completely overlapped with each other,

demonstrating no capacity fading after 10,000 times of charge-discharge.

Using $C=I/m\gamma$ (1), where I is the current, m is the GF weight and γ is the potential scan rate, we obtained a specific capacitance value of 3.5 Fg^{-1} for the 1st and the 10,000th cycle of charging-discharging. This 100% capacity retention and superior consistency rises mainly from the excellent mechanical properties of the GFs and its efficient ion and charge transportation pathways. Built on top of these robust and advantageous features, we endeavour to harness higher capacities and energy densities by mixing GFs with PPY.

In this context, the PPY films were synthesised both chemically and electrochemically on the GFs through Pyrrole oxidation (Figure S4). For chemically prepared composites (under 15 h of polymerization), the PPY content in the PPY-GF composite is found to be ca. 35 wt.%, based on the TGA analysis. We refer to this electrode as PPY-GF in this paper.

Figures 6c to 6f show the CV curves and cycle life of the pure PPY and PPY-GF composite. From Figure 6a to Figure 6c and then to Figure 6e, representing GF, pure PPY and PPY-GF respectively, different CV shapes with increased current values were observed. The low current values of the GF electrode, compared to PPY and PPY-GF, are due to the non-faradic nature of the GF, and to the low density of the as-synthesised graphene foam. However, the GF shows much faster charge-discharge switching than other two electrodes, which is typically carbon electrode behaviour.

Regarding the first CV cycles of the pure PPY and the composite electrode (Figure 6c vs. Figure 6e), the PPY-GF electrode shows higher current values than those of PPY (per the same electrode surface area, and hence higher area capacitance), which is probably due to a combination of parameters: dual charge storage mechanism at the composite electrode, the 3D configuration of the composite (vs. plane architecture of the PPY) and the higher mass loading of the electroactive material per the same electrode surface area.

The cycle life results of pure PPY and PPY-GF are presented in Figures 6d and 6f, respectively. Beginning with PPY, though this electrode shows rectangular CV and good current densities at the first cycle, it cannot maintain these current values at the next cycles and instead there is a gradual decrease in the cyclic performance. From the 1st to the 1,000th cycle, a 30% current reduction was recorded, indicating a possible structural collapse during the repeated charge-discharge tests. In contrast, the composite electrode did not show any current reduction and capacity fading up to 6,000 charge-discharge cycles, as shown in Figure 6f, and even the shape of the CV curves remained almost identical to the initial one. Certainly, this super stability of the electrode arises from the efficient 3D framework which protects the electroactive materials during charge-discharge cycles, thus resulting in 6,000 stable cycles.

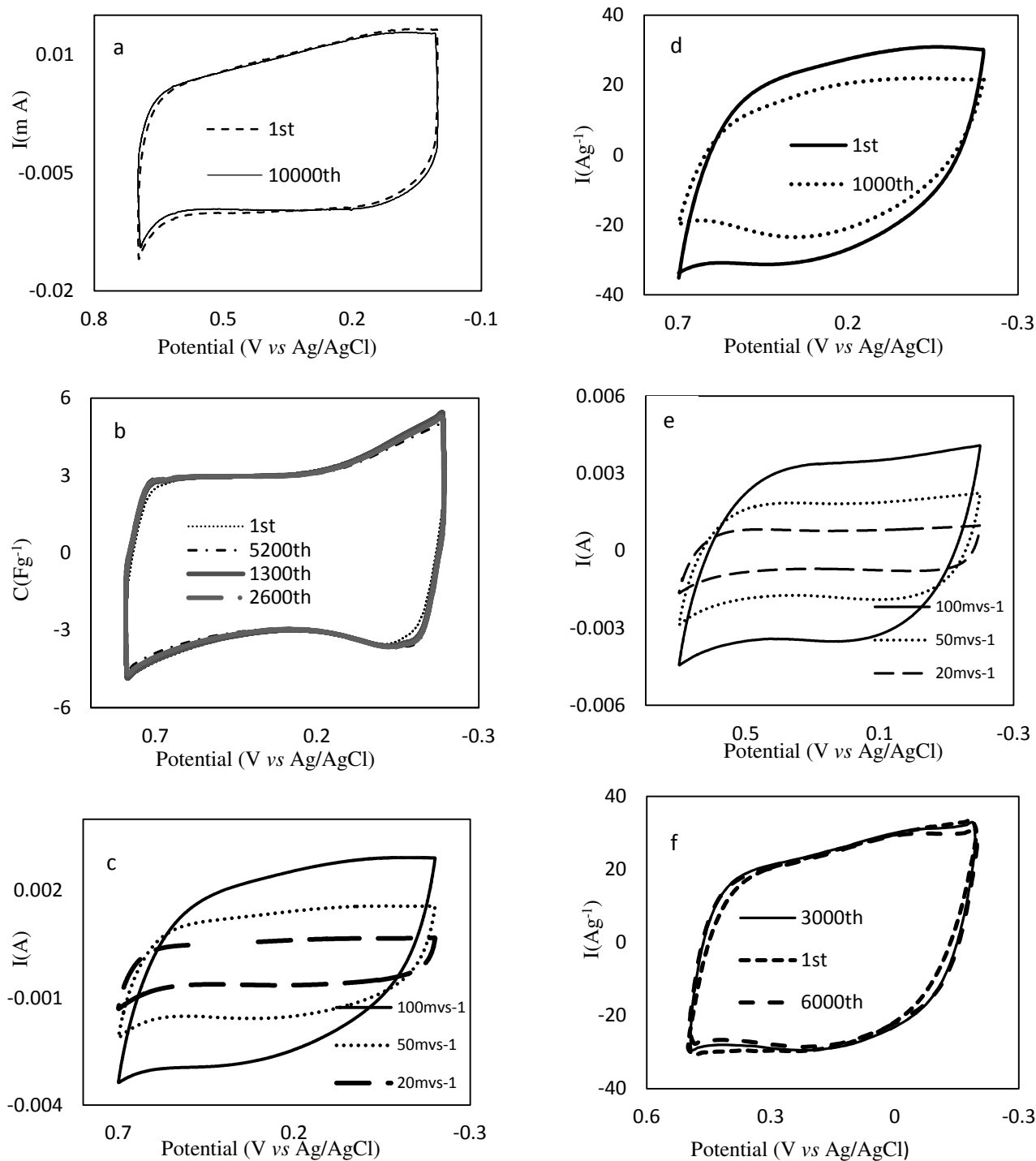


Figure 6: CV curves of different electrodes. (a) the GF at a scan rate of 0.1 Vs^{-1} , (b) the GF capacities at different scans, (c) PPY at different scan rates, (d) PPY at a scan rate of 0.1 Vs^{-1} , (e) PPY-GF at different scan rates, and (f) PPY-GF at a scan rate of 0.1 Vs^{-1} .

The electrodes were further tested by galvanostatic charge-discharge, and the results for the GF, PPY and PPY-GF are shown in Figure 7. The GF electrode (Figure 7a) shows a fast and linear charge-discharge curve, which is the typical behaviour of capacitive materials. The PPY and PPY-GF

electrodes also exhibited linear charge-discharge behaviour. However, for the PPY electrode (Figures 7b) moving from the 1st to 400th cycle, a shorter discharge time and a bigger ohmic drop was recorded for the last cycle, which is indicative of the lower capacitance, more resistive structure and poor mechanical integrity. For the PPY-GF electrode (Figure 7c-e), a much higher charge-discharge time than the GF and also much more stable charge-discharge behaviour (with less IR drop) than the PPY were observed.

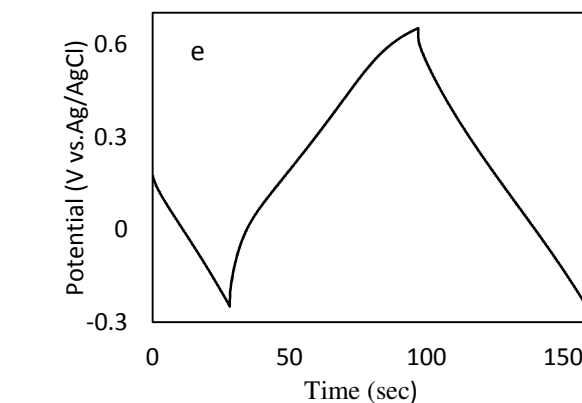
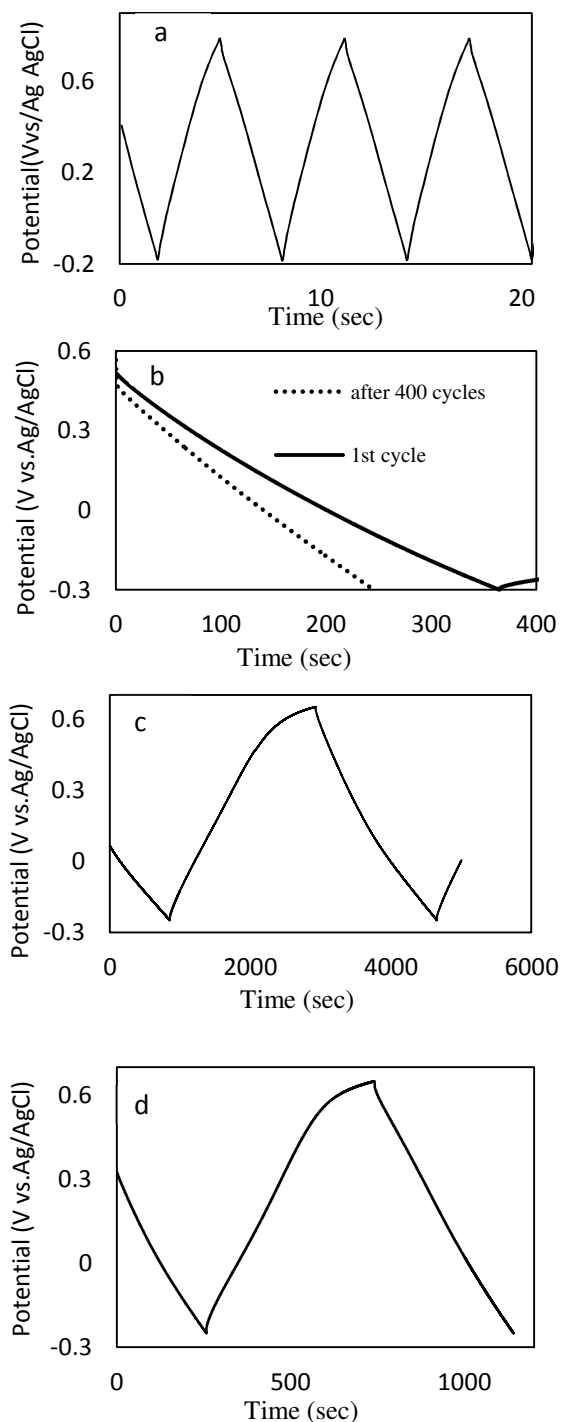


Figure 7: Galvanostatic charge-discharge curves of the GF at 1 Ag⁻¹ (a), PPY at 1 Ag⁻¹ (b), PPY-GF at 0.33 Ag⁻¹ (c), PPY-GF at 1.1 Ag⁻¹ (d), and the PPY-GF at 5.2 Ag⁻¹ (e).

Using the Chronopotentiometry data, the specific capacity, specific energy, specific power and columbic efficiency can be calculated from the following Equations:

$$C_m = \frac{I \times t}{V \times m} \quad (2)$$

$$E = 0.5 CV^2 \quad (3)$$

$$P = \frac{E}{t} \quad (4)$$

$$\varepsilon_c = \frac{t_d}{t_c} \times 100 \quad (5)$$

where, C_m is the specific capacitance, I is the current, V the potential windows, t the discharge time, E the specific energy, P the specific power, ε_c the columbic efficiency, t_d the discharge time and t_c is the charge time. From Equation (2), the maximum specific capacitance values of 660 Fg⁻¹ at 0.34 Ag⁻¹, 570 Fg⁻¹ at 1.1 Ag⁻¹ and 403 Fg⁻¹ at 5.2 Ag⁻¹ were obtained. All electrodes also show very high columbic efficiency. These values are amongst the highest reported capacities, against PPY-graphene, PPY-graphite, and PPY-CNT composite electrodes.^{20,25,27,29-31} Similarly, using Equation (3), a value of 71 Whkg⁻¹ was calculated as the specific energy of the PPY-GF composite. Columbic efficiency of the GF is almost 100% according to Equation (5). Table I summaries the specific energy, specific power and specific capacitance of different samples.

Table 1. Specific Capacitance, Specific Energy and Specific Power of electrodes.

Sample	Capacitance Fg ⁻¹	Energy (Whkg ⁻¹)	Power Wkg ⁻¹	current Ag ⁻¹
GF	3.5	0.44	528	1
PPY	414(1 st cycle)	39	385	1
PPY	265(400 th cycles)	24	390	1
PPY-GF	660	71	150	0.34
PPY-GF	570	63	530	1.1
PPY-GF	403	36	2400	5.2
PPY- GF-E200	560	42	309	1

To further characterise the electrochemical performance of the as-made electrodes, impedance spectroscopy measurements were recorded at the frequency range of 100 kHz - 0.1 Hz (Figure S5). Starting with GF (Figure S5a), this electrode shows higher impedance than other two electrodes, and that is because of the higher conductivity of the PPY and PPY-GF electrode. For both PPY and PPY-GF electrodes, their impedances consist of three parts: the equivalent series resistance (intercept of real impedance) at high frequency (include both solution resistance and contact resistance at the active material/current collector interface), the arc or semicircle part at medium frequencies which is related to the charge transfer process at electrode/electrolyte interface, and the inclined line at low frequencies due to the mass transfer resistance. For the PPY electrode, the straight line at about 45° corresponds to the Warburg impedance which arises from the diffusive charge transport process. Compared with PPY (Figure S5b), the PPY-GF electrode (Figures S5c and S5d) has a much lower series resistance, higher knee frequency and faster diffusion process which are all due to the improved conductivity of the composite electrode. At low frequencies, the impedance plot of the PPY-GF electrode exhibits mainly a high slope straight line which is a characteristic of the capacitive behaviour.

The performance of 3D PPY-GF electrodes prepared under different conditions, such as prepared by 3 h of chemical polymerization (PPY-GF-C3) and electrochemical deposition, was further evaluated, and the results are presented in Figures 8 and 9.

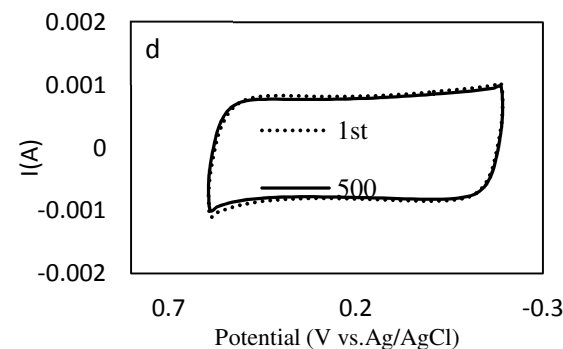
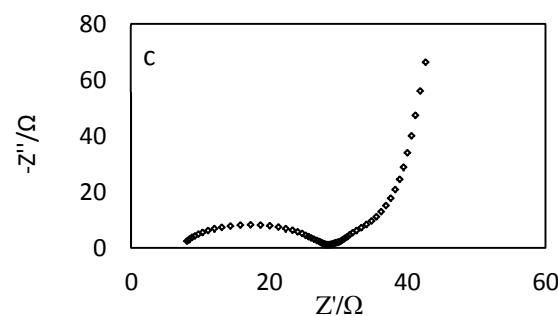
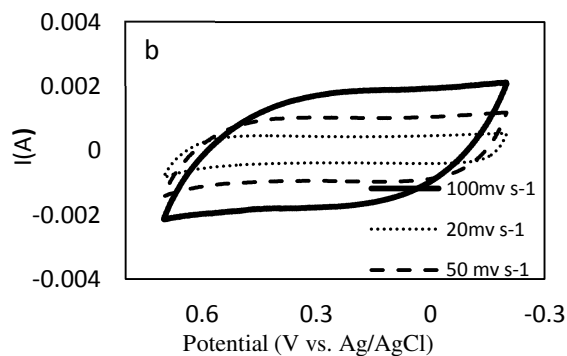
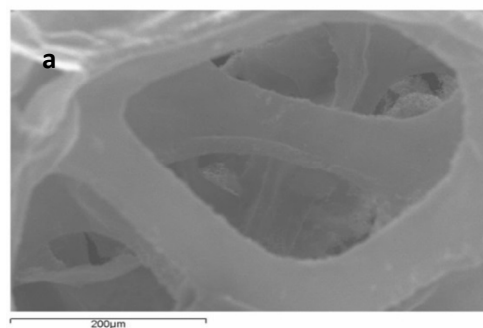


Figure 8: The morphology and electrochemistry characterisation of the PPY-GF-C3 electrode: (a) SEM image, (b) the CV curve, (c) the Nyquist plot at OCP and (d) CV curves showing the cycle stability at a scan rate of 50 mVs⁻¹.

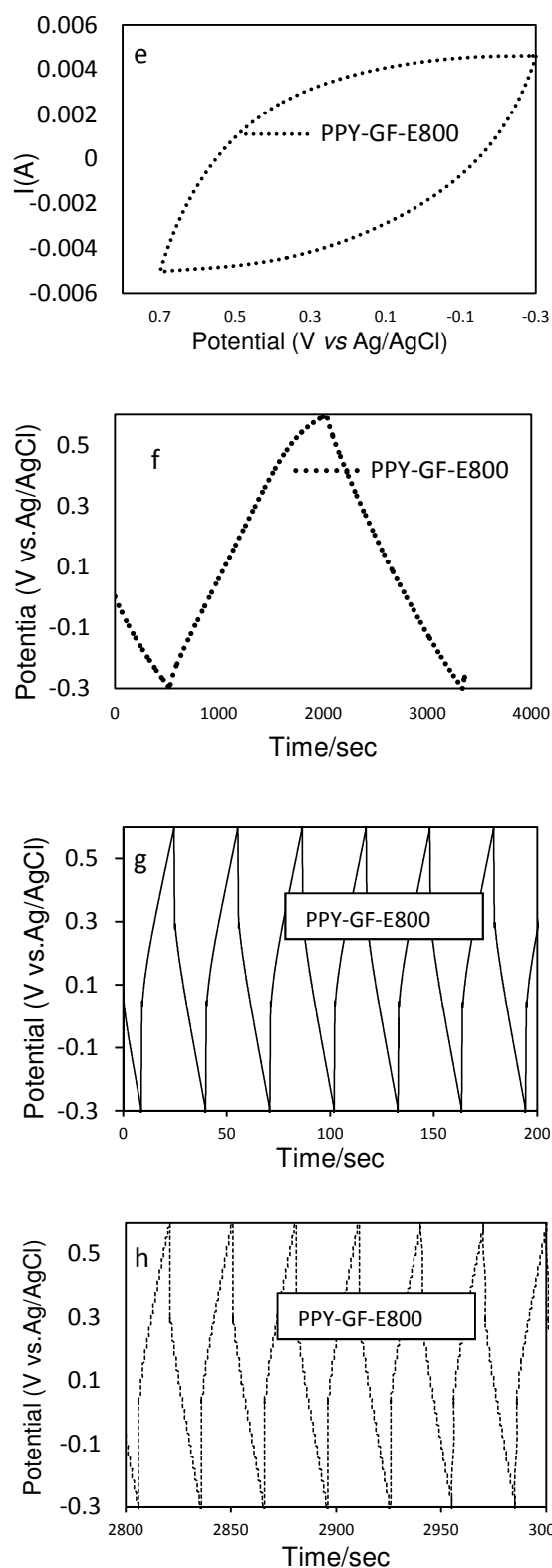
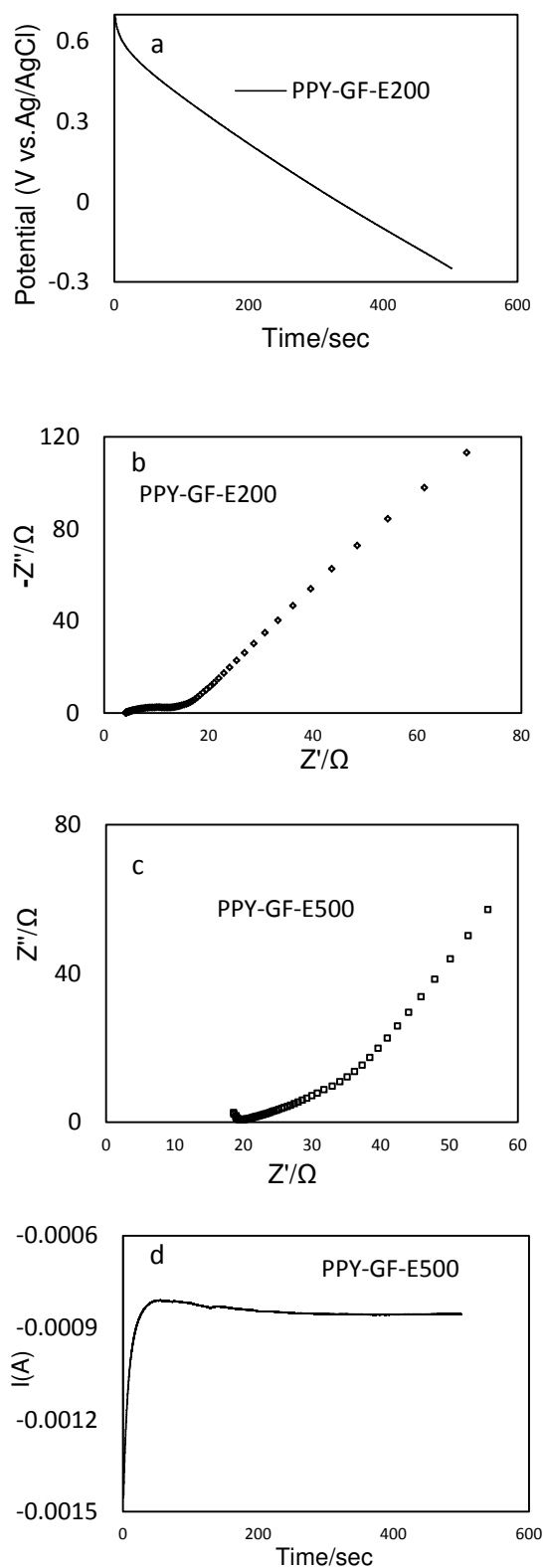


Figure 9: (a) galvanostatic charge-discharge curve of PPY-GF-E200 at 1 Ag^{-1} , (b) the Nyquist plot at OCP of PPY-GF-E200; (c) the Nyquist plot and (d) Chronoamperometry of PPY-GF-E500; (e) the CV curve of the PPY-GF-E800 in 0.5M KCl, (f) the charge-discharge curve of PPY-GF-E800 at 0.0001 A, and (g, h) the charge-discharge results of the PPY-GF-E800 at 0.004 A.

Figure 8 shows the SEM morphology, CV curve and impedance results of PPY-GF-C3 electrode. As expected, the SEM images reveal similar pore distribution as we obtained for the main PPY-GF electrode. Regarding the electrochemical performance, high currents and good rectangular shape were achieved for the CV, indicating a good performance of the electrode. The impedance plot showed a highly sloped straight line at low frequency, and arc-shaped impedance at high frequency, the typical behaviour of pseudocapacitive materials. Phase degree of this electrode is 80° at low frequencies. Compared with the main electrode PPY-GF (prepared under 15 h of chemical polymerization), the PPY-GF-C3 electrode exhibited lower current values and faster charge-discharge cycles, which is possibly due to the lower PPY content in the composite. Indeed, according to our TGA analysis, the PPY content in PPY-GF-C3 is about 20wt%, against 35wt% in PPY-GF. The cycle stability of the PPY-GF-C3 was also assessed by CV and a very good cycle life was observed.

PPY-GF composites prepared by electrodeposition method under 200, 500 and 800 s deposition time were designated as PPY-GF-E200, PPY-GF-E500 and PPY-GF-E800 respectively. Some structural and electrochemical results of these electrodes are shown in Figure 9. Based on the charge-discharge data presented in Figure 9a, a high capacitance of 560 Fg^{-1} (at 1 Ag^{-1}) was recorded for the PPY-GF-E200 electrode, suggesting a high performance for the electrochemically prepared composite. PPY-GF-E200 also has the lowest series resistance (3Ω) among all as-made composite electrodes (Figure 9b). Therefore, high capacitance of the PPY-GF-E200 composite is related mainly to the improved conductivity of this electrode

Electrochemical results of the PPY-GF-E800 electrode are presented in Figure 9(e-h). The charge-discharge curves have a linear shape, representing the capacitive and non-resistive characteristics. Furthermore, the first 500 s and last 500 s of the entire 3000 s charge-discharge process remained the same, and in each 500 s plot the electrode went through 6 cycles of charge-discharge, indicating good cycle stability of the electrode.

Discussion

Highly flexible, binder-free, and hierarchically regulated GF-based 3D electrode structures with excellent cycle life and enhanced pseudocapacitive performance were reported here. The key factors behind the enhanced performance of as-made electrodes are as follows.

Firstly, the high capacity retention behaviour of the GF electrodes after 10,000 cycles is related to the good mechanical stability of the flexible GFs. High compressibility feature of the as-made foam (withstanding up to 75% compression without breakage) demonstrates clearly the suitability of the foam to sustain repeated charge-discharge cycles without losing its initial 3D integrity (See SEM images in Figure S6). As shown in Figure S6, the post-tested pure GF electrode and also the composite electrode retained the same interconnected 3D structure and good integrity (after thousands of cycles) as they had before going through any electrochemical characterisation (Figure 1). In the case of PPY-GF composite, the PPY layers are still closely attached to the GF scaffold after all those cycles, showing excellent contact between GF and PPY and therefore the successful role of the GF as a holder and stabilizer for the PPY coating (Figure S6).

In fact, GFs originated from a highly interconnected 3D structure, built upon strong covalent bonds amongst the carbon atoms of each layer (C-C distance 0.142 nm), even under various curvatures around the pores, make the whole foam very robust and well-connected, and better than any ex-situ constructed 3D carbon structures.

Secondly, the foam density had a significant effect on the flexibility of the GFs, and therefore on the final performance and characteristics of the electrodes. In this study, we have found out that a GF with a high bulk density of 20 mg cm^{-3} had a lower mechanical strength, as well as a lower cycle life, than the GFs with a density value of 3 mg cm^{-3} . At a higher density, the foams had a lower porosity and became more rigid with less flexibility, thus failing to survive the repeated charge-discharge cycle which accompanied constant dimensional (volume) changes. In contrast, at lower density the foam benefits from the open pores which absorbed the mechanical stresses caused during the ion intercalation-extraction process, hence contributing positively to the electrochemical performance of the electrode. The PPY-GF electrodes were prepared both chemically and electrochemically in this work, and both preparation methods gave comparable results. This further indicated that the GF played a more important role than the PPY for the improved performance.

All prepared PPY-GF electrodes benefit from well-connected 3D network. PPY films are bonded non-covalently and mainly through π - π stacking to the GF, though the formation of covalent bonds is also likely to happen at the defective sites of the GF. In the non-covalent bond, the graphene sheets were negatively charged and PPY films were positively charged (p-doped), hence the two components were attached mechanically and electronically together through electrostatic interactions.^{5,6} Regarding graphene π - π stacking, it is notable that whilst such stacking may affect adversely the capacity of the electrode by reducing the accessible surface area of the GF, but π - π interactions between the PPY and GF are helpful in maintaining the stability and integrity of the 3D composite electrode.

Thirdly, another key parameter which affects positively the stability of the electrode and also its high capacitance is the binder free feature of the as-made electrodes. Eliminating binder from electrodes can effectively assist in reducing mechanical stresses of the electroactive materials during ion intercalation and extraction, and can also help in reducing the electrical resistance of the electrode. Therefore, the PPY-GF composite exhibited a remarkably high capacity of 660 Fg^{-1} with excellent capacity retention of 100% after 6,000 cycles, against a *ca.* 30% initial capacity loss after only 1,000 cycles for the pure PPY (Figure 6d). Compared with many recent reports on PPY-carbon composite electrodes, this result displays one of the highest capacitance values.^{20, 25, 27, 29-31, 37}

Another impact of the 3D feature is that growing PPY films on the 3D GF substrate resulted in a more uniform coating of the PPY on the GF (rather than highly agglomerated structure) which affects positively the electrode's conductivity and its electrochemical capacitance.³⁷

At 1.1 Ag^{-1} , the specific capacitance of the composite reached 570 Fg^{-1} which is much higher than the mathematical combination of the PPY and GF ($0.65 \text{ CGF} + 0.35 \text{ CPPY} = 138 \text{ Fg}^{-1}$). The enhanced capacity is believed to arise from several factors: (1) the intrinsic architecture of the interconnected 3D

GFs and the improved conductivity of the PPY-GF (specifically high conductivity of the doped PPY), (2) the synergetic effect between the PPY and GF which formed uniform core-shell 3D structure with adequate PPY thickness; (3) proper pore configuration after the PPY deposition onto the GF and its open porosity structure. Hierarchical 3D architecture of the electrode provides efficient short paths for ion and charge transportation and hence results in a better utilization of the electroactive materials as it facilitates ion (Cl⁻ in this study) interaction with electroactive materials and also via its conductive continuous network accommodate many effective routes for charge transportation and hence energy storage into these composite materials.³⁸ Particularly, macropores assisted in the ions transport, mesopores contributed to both ions and electrons transportation and smaller nano sized pores helped in the charge diffusion process.

To expand our investigation further, we have also prepared 3D PANI-GF composite electrodes, by adopting the same electrochemical deposition method, and identically assessed. As expected, the 3D PANI-GF electrodes demonstrated an excellent cycle life, high capacity and superiority to pure PANI electrodes in all aspects.

Conclusions

We have reported a new 3D-architected, binder-free, and free standing PPY-GF composite electrode which exhibited excellent electrochemical performance with enhanced cyclic stability up to 6,000 cycles. The significantly improved properties are related mainly to the low density, high flexibility, hierarchical structure of the GFs, the redox properties of the PPY, and finally the well-connected 3D core-shell structure of the PPY-GF electrodes. The robust graphitic backbone facilitated efficient charge transfer during the charge-discharge process. Given the binder-free, lack of necessity for current collector, as well as the versatile shape configuration, this 3D electrode architecture is very promising for flexible and lightweight energy storage application. This GF substrate is not only appropriate for the present electrodes, but may also be used in composites for a range of applications where lightweight, flexibility and conductivity are important.

Experimental Section

Methods and materials: GFs were prepared using a Ni foam (supplied by Novamet, USA, with a 99% porosity and 1.6 mm thickness) templated chemical vapour deposition method. Briefly, the Ni template was first annealed for 10 min at 1000°C under H₂ and Ar (total flow rate was 600 sccm), and after that a Styrene (Sigma Aldrich >99%) carbon source was injected at a rate of 0.254 sccm per hour to the furnace for 1 h. After the deposition, the Ni substrate was thoroughly etched overnight in hot 3M HCl (Fisher chemical 37%), to obtain free standing GFs. For the PPY-GF preparation, the as-made GFs were first immersed in a 0.1 M Pyrrole (Alfa Aesar 98%) solution containing methanol (Fisher Chemical >99.5%)/water (50:50 vol%), and then FeCl₃ (Sigma-Aldrich 97%) was added as an oxidant. Subsequently, the resulting solution and the impregnated GF were then left for 15 h (3 h for PPY-GF-C3) at the temperature of 0-5°C, for polymerisation process. Ultimately, the PPY-GFs were then taken out and thoroughly washed with distilled water. The volume ratio of Pyrrole solution to FeCl₃ oxidant was 1:2. For comparison, pure PPY films and PPY-GF-E were also prepared electrochemically from the 0.1 M Pyrrole solution at different deposition times.

Measurements: SEM and EDS tests were conducted using an Hitachi S3200N SEM-EDS equipment. XRD powder diffraction patterns were recorded using a Bruker D8 Advance diffractometer working with a Cu-K α radiation ($\lambda = 0.154$ nm) operated at 40 kV and 40 mA. Thermal gravimetric analysis was performed using a TA SDT Q600 TGA-DSC instrument, at a ramping rate of 10°C per min under air environment. The Raman spectra were obtained using a Renishaw inVia Raman microscope. The excitation laser beam at a wavelength of 532 nm was focused by a 50 \times objective onto a small area of the sample. TEM experiments were performed on a JEM-2100 TEM, operated at 200 kV. For the TEM sample preparation, GF and PPY-GF samples were ultrasonically dispersed in acetone (Fisher Chemical) for 30 min and then the suspension was dropped onto a holey carbon coated copper grid (300 mesh, Agar). Mechanical properties were assessed using an assembled tensile testing machine (Figure 5a). Electrochemical tests were carried out using a CHI 660C Electrochemical Workstation and a three electrode cell: Pt as the auxiliary electrode, Ag/Ag Cl as the reference electrode and gold as the working electrode (2 mm diameter), in a 0.5 M KCl (Sigma-Aldrich 99-100 %) electrolyte. Impedance measurements were recorded in the frequency range of 100 kHz-0.1 Hz at OCP with voltage amplitude of 0.005 V.

Acknowledgement

Thank the University of Exeter for financial support.

Notes and references

^a College of Engineering, Mathematics and Physical Sciences, University of Exeter, Exeter EX4 4QF, UK

E-mail: Y.Zhu@exeter.ac.uk

^b Faculty of Science and Engineering, The University of Nottingham Ningbo Campus, Ningbo, 315100, China

† Electronic Supplementary Information (ESI) available: [details of any supplementary information available should be included here]. See DOI: 10.1039/b000000x/

- 1 P. Simon, Y. Gogotsi, B. Dunn, *Science*. 2014, **343**, 1210
- 2 J. W. Long, B. Dunn, D. R. Rolison, H. S. White, *Chem. Rev.* 2004, **104**, 4463
- 3 K. Edström, D. Brandell, T. Gustafsson, *Interface*. 2011, **20**, 41
- 4 Y. Yu, C. Yan, L. Gu, X. Lang, K. Tang, *Adv. Energy Mater.* 2013, **3**, 281
- 5 S. Chabi, C. Peng, D. Hu, Y. Zhu, *Adv. Mater.* 2014, **26**, 2440
- 6 H. Zhang, X. Yu, P. V. Braun, *Nat. Nano Technol.* 2011, **6**, 277
- 7 S. K. Lee, K. Rana, J. H. Ahn, *J. Phys. Chem. Lett.* 2013, **4**, 83
- 8 J. H. Pikul, H. G. Zhang, J. Cho, P. V. Braun, W. P. King, *Nat. Commun.* 2013, **4**, 1732
- 9 N. Li, Z. Chen, W. Ren, F. Li, H. M. Cheng, *Proc Natl Acad Sci.* 2012, **109**, 17360

- 10 C. S. Choi, Y. U. Park, H. Kim, N. R. Kim, K. Kang, H. M. Lee, *Electrochim Acta*. 2012, **70**, 98
- 11 X. Yu, B. Lu, Z. Xu, *Adv. Mater.* 2014, **26**, 1044
- 12 H. Wang, H. S. Casalongue, Y. Liang, H. Dai, Wang, H., J. Am. Chem. Soc. 2010, **132**, 7472.
- 13 H. Ji, L. Zhang, M. T. Pettes, H. Li, S. Chen, L. Shi, R. Piner, R. S Ruoff, *Nano Lett.* 2012, **12**, 2446
- 14 K. Xi, P.R. Kidambi, R. Chen, C. Gao, X. Peng, C. Ducati, S. Hofmann, R.V. Kumar, *Nanoscale*.2014, **6**, 5746.
- 15 J. Ji, L.L. Zhang, H. Ji, Y. Li, X. Zhao, X. Bai, X. Fan, F. Zhang, R. S. Ruoff, *ACS Nano*. 2013, **7**, 6237
- 16 C. John, R. Fritzsche, A. Ignaszak, *Electroanalysis*. 2014, **26**, 1560
- 17 D. R. Rolison, J. W. Long, J. C. Lytle, A. E. Fischer, C. P. Rhodes, T. M. McEvoy, M. E. Bourg, L. M. Lubers, *Chem. Soc. Rev.* 2009, **38**, 226
- 18 Y. Liu, W. Zhang, Y. Zhu, Y. Luo, Y. Xu, A. Brown, James N. Culver, C. A. Lundgren, K. Xu, Y. Wang, C. Wang, *Nano Lett.* 2012, **13**, 293
- 19 J. Guo, X. Chen, C. Wang, *J. Mater. Chem.* 2010, **20**, 5035
- 20 H. H. Chang, C. K. Chang, Y. C. Tsai, C. S. Liao, *Carbon*, 2012, **50**, 2331
- 21 S. Sahoo, S. Dhibar, C. Das, *Express Polymer Lett.* 2012, **6**, 965
- 22 R. Ansari, *Journal of Chemistry*. 2006, **3**, 186
- 23 S. Sadki, P. Schottland, N. Brodie, G. Sabouraud, *Chem. Soc. Rev.* 2000, **29**, 283
- 24 Y. Liu, H. Wang, J. Zhou, L. Bian, E. Zhu, J. Hai, J. Tang, W. Tang, *Electrochim. Acta*. 2013, **112**, 44
- 25 P. A. Basnayaka, M.K. Ram, L. Stefanakos, A. Kumar, *Graphene*. 2013, **2**, 81
- 26 C. Peng, S. Zhang, D. Jewell, G.Z. Chen, *Prog. Nat. Sci.* 2008, **18**, 777
- 27 S. Bose, N.H. Kim, T. Kuila, K. Lau, J.H. Lee, *Nanotechnology*, 2011. **22**, 295202
- 28 T. Liu, L. Finn, M. Yu, H. Wang, T. Zhai, X. Lu, Y. Tong, Y. Li, *Nano Lett.*, 2014, **14**, 2522
- 29 J.H. Park, J.M. Ko, O.O. Park, D.W Kim, *J. Power Sources*. 2002, **105**, 20
- 30 A. Singh, A. Chandra, *J. Appl. Electrochem.* 2013, **43**, 773
- 31 D. Zhang, Q. Q. Dong, X. Wang, W. Yan, W. Deng, L. Y. Shi, *J. Phys. Chem. C*.2013, **117**, 20446
- 32 Z. Chen, W. Ren, L. Gao, B. Liu, S. Pei, H.M. Cheng, *Nat. Mater.* 2011, **10**, 424
- 33 X. Li, A. Dhanabalan, L. Gu, C. Wang, *Adv. Energy Mater.* 2012, **2**, 238
- 34 A. C. Ferrari, *Solid State Commun.* 2007, **143**, 47
- 35 T. Hasan, V. Scardaci, P. H. Tan, F. Bonaccorso, A. G. Rozhin, Z. Sun, A. C. Ferrari, *Nanotube and graphene polymer composites for photonics and optoelectronics*, in *Molecular-and Nano-Tubes*, (Eds: O. Hayden, K. Nielsch), Springer, 2011, Ch 9
- 36 Y. Sun, G. Shi, *J. Polym. Sci., Part B: Polym. Phys.* 2013, **51**, 231
- 37 Z. Chen, D. Yu, W. Xiong, P. Liu, Y. Liu, L. Dai, *Langmuir*. 2014, **30**, 3567
- 38 Y. Meng, K. Wang, Y. Zhang, Z. Wei, *Adv. Mater.* 2013, **25**, 6985